

Molecular effects in investigations of tritium molecule β decay endpoint experiments

Natasha Doss* and Jonathan Tennyson

Department of Physics and Astronomy, University College London, Gower Street, WC1E 6BT London, United Kingdom

Alejandro Saenz

AG Moderne Optik, Institut für Physik, Humboldt-Universität zu Berlin, Hausvogteiplatz 5-7, D-10 117 Berlin, Germany

Svante Jonsell

Department of Physics, Umeå University, SE-90187 Umeå, Sweden

(Received 8 July 2005; published 17 February 2006)

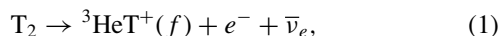
The final state distribution of the first six electronic states of ${}^3\text{HeT}^+$, ${}^3\text{HeD}^+$ and ${}^3\text{HeH}^+$ resulting from the β decay of T_2 , DT , and HT are calculated, to satisfy the higher-resolution requirements and increased sensitivity of the future tritium neutrino mass experiments. The sensitivity of the initial temperature, ortho-para ratio, and isotopic composition of the source is considered. Estimates of the error in the value of the neutrino mass deduced from fitting, due to uncertainties in the temperature, the ortho-para ratio of T_2 , and the percentage of DT molecules in the source are presented.

DOI: [10.1103/PhysRevC.73.025502](https://doi.org/10.1103/PhysRevC.73.025502)

PACS number(s): 31.15.-p, 14.60.Pq, 23.40.Bw

I. INTRODUCTION

The most promising direct experiments for determining the neutrino mass are based on the study of the β decay of molecular tritium:



where f refers to the molecular state of the ${}^3\text{HeT}^+$ molecule.

The idea is to detect the energies of the electrons created in the decay and to deduce the mass of the electron antineutrino, $m_{\bar{\nu}_e}$, by analyzing the β spectrum. As the intensity of β electrons near the endpoint is very weak and their detection is hampered by background noise, an exact value for the endpoint energy, the maximum β electron energy, is difficult to obtain. Instead $m_{\bar{\nu}_e}$ must be obtained by analyzing the shape of the β spectrum close to the endpoint, where the effect of a nonzero neutrino mass is greatest. The shape of the β spectrum is dependent on the distribution of energy released in excitations of the daughter molecule, ${}^3\text{HeT}^+$.

There were extensive calculations of the final state distribution of ${}^3\text{HeT}^+$ in the 1980's [1–7]. However, the contemporaneous experiments reported negative values for the neutrino mass squared, $m_{\bar{\nu}_e}^2$, obtained from fitting the experimental results to theoretical spectra, that lay outside the error bars extending into the negative region. This indicated that there was some systematic error in the experiment or the adopted theory. Because of this and also the increasing sensitivity of the experiments, a reinvestigation of the final state distribution was performed in the 1990's [8–15]. Special emphasis was placed on validating the underlying approximations used in the previous calculations. The validity of the sudden approximation was demonstrated by Saenz and Froelich [12], having found that the corrections to it, which were calculated explicitly, were negligible. The effect of electronic excitation

through recoil was also found to be negligible [11]. Jonsell *et al.* [13,14] investigated the nonadiabatic effects (the coupling of the electronic and nuclear motions) and found them to be very small, therefore validating the Born-Oppenheimer approximation. An important change that was made was the relativistic correction to the recoil momentum, which increases the recoil momentum by 1% [14]. Most of the other refinements concentrated on the less accurately known electronic continuum of ${}^3\text{HeT}^+$ [8]. However, the negative mass squared problem remained in the experiments of the 1990's.

The most recent neutrino mass experiments to be performed were the Mainz [16] and Troitsk [17] experiments that ran from 1994 to 2001. Both experiments reported negative $m_{\bar{\nu}_e}^2$ from the analysis of their early runs. Each group analyzed the systematic effects and made improvements to their experimental setups and $m_{\bar{\nu}_e}^2$ fitting procedures. The Troitsk group associated the negative $m_{\bar{\nu}_e}^2$ problem with existence of an excess count rate located a few electron volts below the endpoint, the ‘Troitsk anomaly.’ Taking the bump into account with the addition of a steplike function, with variable height and position, to the theoretical spectrum resulted in values of $m_{\bar{\nu}_e}^2$ compatible with zero, thus eliminating the negative value problem. In the Mainz experiment the main systematic uncertainties were connected to the physics and properties of the quench-condensed tritium source. By reducing these uncertainties and by the lowering and stabilization of the background rate, the Mainz runs of 1998–2001 also reported values of $m_{\bar{\nu}_e}^2$ compatible with zero. The experiments at Mainz and Troitsk reported upper limits for the mass of $m_{\bar{\nu}_e} < 2.3$ eV [18] and $m_{\bar{\nu}_e} < 2.05$ eV [19], respectively. Several neutrino oscillation experiments have shown that oscillations between different neutrino flavors do occur, implying that the neutrino mass is nonzero. Unfortunately these oscillation experiments are not sensitive to the neutrino masses directly; however, their evidence for massive neutrinos provides motivation for a next-generation tritium β decay experiment.

*Electronic address: natasha@theory.phys.ucl.ac.uk

The future KATRIN experiment [20,21] anticipates a sensitivity on the neutrino mass of $m_{\bar{\nu}_e} < 0.2$ eV (90% C.L.), a factor of 10 higher sensitivity compared with the Mainz and Troitsk experiments. The experiment will be performed by using a gaseous molecular tritium source at a temperature of 27 K. It will use an estimated 95% isotopic purity, with the main contamination coming from deuterium. This increased sensitivity and changes in requirements for the KATRIN experiment has therefore led to a reinvestigation of the molecular effects in the experiment. A calculation of the final state distribution of the six lowest electronic states of ${}^3\text{HeT}^+$, ${}^3\text{HeD}^+$, and ${}^3\text{HeH}^+$ has been performed, and the results are reported here. The calculation is so far limited to these states only, as the aim of KATRIN is to obtain the neutrino mass by analyzing the β spectrum in an energy interval with a lower limit of 30 eV below the endpoint energy [22]. As the effects of the Rydberg states and the electronic continuum of ${}^3\text{HeT}^+$ start at 40 eV below the endpoint [15], these have not been reinvestigated. The emphasis of these new calculations is to investigate the effect of the uncertainty in temperature of the T_2 source and isotope contamination on the deduced value of the neutrino mass obtained from fitting.

II. THEORY

A. β spectrum

An expression for the intensity $I(E_e)$ of β electrons, with kinetic energy E_e and momentum p_e , can be derived from Fermi theory. Detailed nonrelativistic derivations (except for a relativistic relation between the energy and momentum of the β electron and the neutrino) are given by Szalewicz *et al.* [5] and Saenz and Froelich [11].

Results from neutrino oscillation experiments have provided compelling evidence for non-zero neutrino masses. Observations show that while traveling from the source to the detector, a neutrino flavor eigenstate, e.g., a muon neutrino, can transform into another flavor eigenstate, e.g., an electron neutrino. The existence of these neutrino oscillations requires a nontrivial mixing between the neutrino flavor eigenstates (ν_e, ν_μ, ν_τ), produced in weak interactions and the corresponding mass eigenstates (ν_1, ν_2, ν_3) via a unitary mixing matrix U . They also require that the mass eigenvalues (m_1, m_2, m_3) differ from one another and hence must be nonzero. Taking into account the different mass states, the expression for the intensity of β electrons is given by

$$I(E_e) = AF(p_e)p_e(E_e + m_e c^2) \sum_{fj} \{ P_f(W_0 - E_f - E_e) \times H(W_0 - E_f - E_e - m_{\nu_j} c^2) |U_{ej}|^2 \times [(W_0 - E_f - E_e)^2 - m_{\nu_j}^2 c^4]^{1/2} \}, \quad (2)$$

where

$$W_0 = m_{\text{T}_2} + E_0^{\text{T}_2} - m_{{}^3\text{HeT}^+} - E_0^{{}^3\text{HeT}^+} - m_e c^2 - E_{\text{rec}}. \quad (3)$$

A is a normalization constant, $F(p_e)$ is the Fermi function, and H is the Heaviside step function ensuring that the intensity is real. E_f is the energy of the final molecular state f of ${}^3\text{HeT}^+$, and P_f is the probability that the ${}^3\text{HeT}^+$ ion will be left in state f after the β decay. The distribution of P_f and E_f is known as

the molecular final state distribution (which is abbreviated as FSD throughout this paper). Here m_{T_2} , $m_{{}^3\text{HeT}^+}$, and m_e are the masses of the parent molecule, daughter molecule, and electron respectively; $E_0^{\text{T}_2}$ and $E_0^{{}^3\text{HeT}^+}$ are the ground state energies of the molecules, and E_{rec} is the recoil energy transferred to the center of mass motion of the molecular system. Hence, W_0 is the maximum kinetic energy of the β electron if the neutrino mass were zero. The conservation of momentum will be discussed in the next section.

For a quasi-degenerate model of the neutrino masses ($m_1 \approx m_2 \approx m_3$), we can parametrize the analysis of the β spectrum by Ref. [18]

$$m_{\nu_e}^2 = \sum_{j=1}^3 |U_{ej}|^2 m_{\nu_j}^2, \quad (4)$$

where m_{ν_e} is the effective electron antineutrino mass. However, for a heirarchical ordering of the neutrino masses ($m_1 \ll m_2 \ll m_3$), the three mass eigenstates and also the mixing angles and CP phases that characterize the mixings must be taken into account, resulting in several more independent fit parameters. The effects of mixing result in the following modifications of the β spectrum (see Ref. [22]): (1) the β spectrum will have an experimental endpoint energy $E = W_0 - m_1$ (where m_1 is the lightest mass eigenstate), and (2) kinks will appear at energies $E^i \approx W_0 - m_i$ (where the magnitude of the kinks are determined by $|U_{ei}|^2$).

The mass of the neutrino is obtained by fitting the experimental data to theoretical spectra given by Eq. (2). P_f and E_f are obtained from theory, while A , W_0 , and m_{ν}^2 (as well as the background rate) are free parameters.

Different final quantum states of the ${}^3\text{HeT}^+$ ion give rise to separate branches of the β spectrum, each with a different endpoint energy. For the total β spectrum a sum over all final states is performed as in Eq. (2). A very accurate knowledge of the FSD, including nuclear motion effects, is crucial in the determination of the neutrino mass from the β spectrum, as the accuracy of the neutrino mass is limited by the accuracy of the FSD. The effect of different levels of accuracy of the FSD on the β spectrum is shown by Fackler *et al.* [2]. This is one of the reasons that T_2 is the source of choice. It is one of the simplest tritium-containing compounds, and for both T_2 and ${}^3\text{HeT}^+$ high-accuracy quantum chemical computations can be performed and reliable energies and probabilities calculated.

B. Molecular excitations in the β decay process

The theory of the molecular β decay process is given by Cantwell [23], where an expression for the probability of molecular excitations of the daughter ion is derived from the Fermi golden rule formula.

If the sudden approximation (a complete neglect of the interaction between the β electron and the remaining molecular ion) is assumed, the probability that the daughter ion ${}^3\text{HeT}^+$ will be in a final state f following the β decay of a T_2 molecule in an initial state i is

$$P_{if} = \left| \langle \Psi_f^{{}^3\text{HeT}^+} | e^{i\mathbf{K}\cdot\mathbf{R}} | \Psi_i^{\text{T}_2} \rangle \right|^2, \quad (5)$$

where $\Psi_f^{3\text{HeT}^+}$ and $\Psi_i^{\text{T}_2}$ are the wave functions describing the quantum states of the daughter and parent molecule, respectively, and the exponential $e^{i\mathbf{K}\cdot\mathbf{R}}$ arises from the recoil of the β electron. $\mathbf{K} = -\mathbf{p}_e m_T / (m_T + m_{\text{He}} + 2m_e)\hbar$, and \mathbf{R} is the internuclear distance. The derivation of \mathbf{K} and an estimate of the effect of the approximation when \mathbf{R} is used is given by Saenz and Froelich [11].

A further approximation that we have made is the use of a constant recoil energy. The recoil energy, E_{rec} [see Eq. (2)], for T_2 is 1.72 eV for an 18.6 keV (the maximum β electron energy) electron. The dependence of the recoil energy on the momentum of the neutrino is negligible. For a 1 eV neutrino the recoil energy would change by a factor of 10^{-5} . A larger effect results from the neglect of the dependence of the recoil energy on the β electron energy. However, in the region close to the endpoint where the fit is to be performed this error is still negligible. For the recoil momentum that enters into the final state equation [Eq. (5)] we have also neglected the dependence on the neutrino momentum and the change in electron momentum. This effect has also been shown [14] to be very small.

If we consider transitions to bound rovibrational states of $^3\text{HeT}^+$, for the case where the initial T_2 molecule is in its ground electronic and rovibrational state ($n_i = 1$, $v_i = 0$, $J_i = 0$, $M_i = 0$), where n , v , J , and M are the electronic, vibrational, rotational, and azimuthal quantum numbers, Eq. (5) reduces to (see the Appendix)

$$P_{nvJ} = (2J + 1) \left| \int_0^\infty S_n(R) j_J(KR) f_{nvJ}^f(R) f_{100}^i(R) dR \right|^2, \quad (6)$$

where f_{nvJ}^f/R and f_{100}^i/R are the radial parts of the rovibrational wave functions of $^3\text{HeT}^+$ and T_2 , $S_n(R)$ is the overlap of the electronic wave functions of $^3\text{HeT}^+$ and T_2 , and $j_J(KR)$ is the spherical Bessel function.

For transitions to the nuclear motion continuum, Eq. (6) will not be dependent on v . The probability per unit energy $P_{nJ}(E)$ that the $^3\text{HeT}^+$ molecule dissociates via the n th electronic state and that the dissociation products are in a state with energy E and angular momentum J , as shown by Jeziorski *et al.* [3], is given by

$$P_{nJ}(E) = (2J + 1) \times \left| \int_0^\infty S_n(R) j_J(KR) f_{nJ}^f(R|E) f_{100}^i(R) dR \right|^2, \quad (7)$$

where $f_{nJ}^f(R|E)$ are the energy normalized radial functions of the continuous spectrum.

III. CALCULATION OF THE FINAL STATE DISTRIBUTION

A. Transitions to the electronic ground state of $^3\text{HeT}^+$

The radial or (effective) one-dimensional Schrödinger equation is

$$-\frac{\hbar^2}{2\mu} \frac{d^2 f_{nvJ}(R)}{dR^2} + U_{nJ}^{\text{eff}}(R) f_{nvJ}(R) = E_{nvJ} f_{nvJ}(R), \quad (8)$$

where μ is the effective or reduced mass of the system and E_{nvJ} the energy of the rovibrational state. The effective one-dimensional potential, $U_{nJ}^{\text{eff}}(R)$,

$$U_{nJ}^{\text{eff}}(R) = \frac{J(J+1)\hbar^2}{2\mu R^2} + U_{\text{BO}}(R) + U_{\text{ad}}(R) + U_{\text{rel}}(R) + U_{\text{rad}}(R), \quad (9)$$

is a sum of the centrifugal term, the electronic potential in the nonrelativistic Born-Oppenheimer approximation $U_{\text{BO}}(R)$, and if known, the mass-dependent adiabatic $U_{\text{ad}}(R)$, relativistic $U_{\text{rel}}(R)$, and radiative $U_{\text{rad}}(R)$ corrections.

The transition probabilities were calculated by using Le Roy's programs LEVEL [24] and BCONT [25], with modifications made to them; LEVEL, which solves the radial Schrödinger equation [Eq. (8)] for bound and quasi-bound levels by numerical integration, was used to calculate energies, wave functions and probabilities of the bound rovibrational states and of the predissociative resonances, including widths for the resonances. BCONT, which calculates bound-continuum transition intensities, was used to calculate probability density distributions for each J in the nuclear motion continuum at chosen energy steps.

To obtain the ground state electronic energy potential of $^3\text{HeT}^+$, we used the same procedure as in Ref. [14]. We used the Born-Oppenheimer potentials from Refs. [26–28] and the adiabatic correction from Ref. [28]. Two extra points at $R = 0.6$ and 0.8 a.u. were obtained by extrapolating the adiabatic correction.

The ground state electronic energy potential of T_2 was obtained by using the Born-Oppenheimer potential and the radiative, relativistic and adiabatic corrections from Ref. [29]. The electronic overlap $S_1(R)$ of Ref. [1] was used.

In the previous calculation of the FSD [14], the nuclear reduced masses were used for the molecules when the radial Schrödinger equation was solved in LEVEL and BCONT. Coxon and Hajigeorgiou [30] investigated the effect of using different reduced masses for the isotopes of HeH^+ . We have tested, for $^3\text{HeH}^+$ and $^3\text{HeD}^+$, the use of the four different reduced masses as in Ref. [30]; the nuclear reduced mass μ_{nuc} , the charge adjusted reduced mass μ_{C} , the dissociation reduced mass μ_{dis} and the effective mass μ_{eff} (which assumes that one of the two electrons is essentially tied to the He^{2+} nucleus, with the second electron being distributed between the H^+ and He^+ centers). The energies of the rovibrational states, obtained by the LEVEL program using each of the reduced masses, were compared with experimental transition frequencies given in Refs. [31–33]. Our results are summarised in Table I. μ_{eff} was found to be the best compromise (as in Ref. [30]) and so was used for the daughter molecular ion in our calculations. However, at the level of a few tenths of an electron volt, the energy resolution of KATRIN, the choice of reduced mass has no effect on the FSD. Similar calculations have recently been used to determine the partition function and opacity of various HeH^+ isotopologues for stellar modeling [34]; these used μ_{dis} .

Predissociative resonances in the region 0–0.5 eV above the dissociation limit of $^3\text{HeT}^+$, result in volatile behavior of the probability. For this reason, the probability density

TABLE I. Differences between experimental rotation-vibration transition frequencies (cm^{-1}) [31–33] and theoretical frequencies calculated by using different reduced masses for ${}^3\text{HeH}^+$ and ${}^3\text{HeD}^+$

(v', J')	(v'', J'')	ν_{obs}	$\nu_{\text{calc}} - \nu_{\text{obs}}$			
			μ_{nuc}	μ_{C}	μ_{dis}	μ_{eff}
${}^3\text{HeH}^+$						
(0,1)	(0,0)	71.367	0.004	-0.042	-0.005	-0.016
(0,2)	(0,1)	142.293	0.005	-0.084	-0.008	-0.033
(1,0)	(0,1)	2923.680	0.395	-0.408	0.279	0.050
(1,1)	(0,2)	2846.775	0.389	-0.365	0.281	0.066
(1,2)	(0,3)	2764.768	0.388	-0.311	0.288	0.088
(1,3)	(0,4)	2678.113	0.383	-0.258	0.291	0.108
(1,4)	(0,5)	2587.243	0.380	-0.200	0.297	0.131
(1,5)	(0,6)	2492.591	0.372	-0.143	0.298	0.151
(1,1)	(0,0)	3060.433	0.399	-0.488	0.270	0.018
(1,2)	(0,1)	3119.405	0.400	-0.519	0.268	0.006
(1,3)	(0,2)	3171.549	0.402	-0.542	0.266	-0.003
(1,4)	(0,3)	3216.468	0.403	-0.559	0.265	-0.009
(1,5)	(0,4)	3253.785	0.406	-0.567	0.267	-0.011
(1,6)	(0,5)	3283.156	0.404	-0.572	0.264	-0.014
(1,7)	(0,6)	3304.247	0.395	-0.575	0.256	-0.021
(1,8)	(0,7)	3316.761	0.395	-0.560	0.258	-0.014
(6,12)	(5,11)	981.322	0.014	1.380	0.210	0.600
${}^3\text{HeD}^+$						
(0,2)	(0,1)	89.932	0.006	-0.031	-0.007	-0.011
(0,3)	(0,2)	134.467	0.009	-0.046	-0.011	-0.016
(1,0)	(0,1)	2378.374	0.374	-0.071	0.219	0.171
(1,2)	(0,3)	2280.081	0.378	-0.025	0.238	0.194
(1,2)	(0,1)	2504.487	0.386	-0.109	0.213	0.160
(1,3)	(0,2)	2540.161	0.391	-0.116	0.214	0.159
(1,4)	(0,3)	2572.388	0.392	-0.126	0.212	0.155
(1,5)	(0,4)	2601.007	0.396	-0.129	0.213	0.156
(6,19)	(5,18)	1034.144	0.048	0.738	0.289	0.363
(7,17)	(5,19)	995.415	0.061	1.215	0.464	0.589

distributions of nonisolated resonances and those with sufficiently large widths, were obtained by using the BCONT program and very small energy steps (as small as 10^{-9} eV). However, for very narrow resonances this step size is still too large, and the resonances could not be characterized by using the BCONT program. In these cases the energy and total probability associated with the resonance given by the bound-bound transition program LEVEL was used. For the region beyond 0.5 eV above the dissociation limit, where no resonances are present, an energy step of 0.001 eV is sufficient.

The previous FSD [15] was presented as a finite number of discrete transition probabilities by dividing the spectrum into small bins varying in size from 0.1 eV, for the ground state of ${}^3\text{HeT}^+$, to 1.0 eV, for the electronically excited states of ${}^3\text{HeT}^+$. This approach is the best for analysis of the experiments and was also used here. However, due to the improved sensitivity of the experiment, 0.1 eV bins are no longer sufficient, and so 0.01 eV bins are used throughout.

The FSD for the electronic ground state is shown in Fig. 1, where the energy zero is the ground rovibrational state of ${}^3\text{HeT}^+$. Due to the energy resolution of the experiment, such

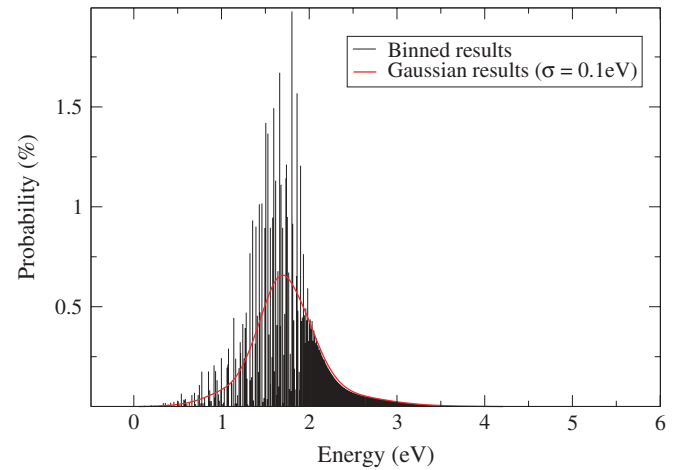


FIG. 1. (Color online) Final state probability distribution (0.01 eV bins) for calculations to the electronic ground state of ${}^3\text{HeT}^+$.

fine energy bins cannot be resolved. To illustrate the shape of the distribution we have assumed an experimental energy resolution of $\sigma = 0.1$ eV and produced a Gaussian average (in terms of probability density) of the unbinned results. This probability density distribution was integrated over bins of 0.01 eV and is also shown in Fig. 1.

B. Electronically excited states of ${}^3\text{HeT}^+$

The Born-Oppenheimer energies and electronic overlaps $S_n(R)$ of the first five electronically excited states of ${}^3\text{HeT}^+$ were taken from Ref. [14]. No adiabatic corrections were included. These excited states are essentially dissociative, and therefore only the BCONT program was used. The $n = 2, 4,$ and 5 states dissociate to $\text{He}^+ + \text{T}$, and the $n = 3$ and 6 states dissociate to $\text{He} + \text{T}^+$. For the excited states, the relevant dissociation reduced mass was used instead of the effective reduced mass. The probability distribution for the $n = 2-6$ states is shown in Fig. 2 for energy bins of 0.01 eV.

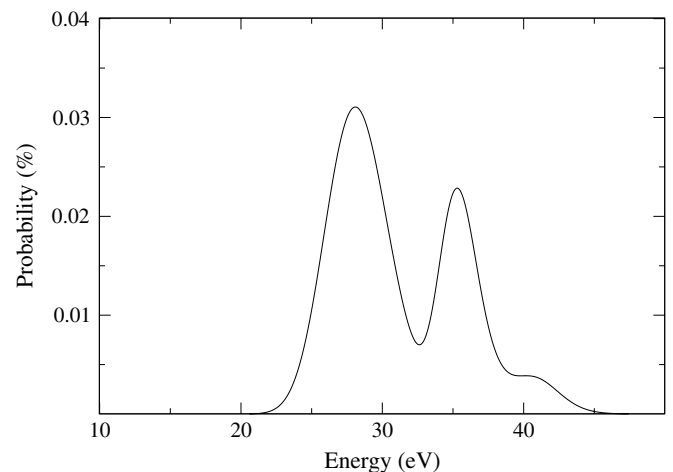


FIG. 2. Final state probability distribution (0.01 eV bins) for the first five electronically excited states of ${}^3\text{HeT}^+$.

C. Rotational excitation of T_2

If the experiments are performed with a source at a temperature greater than 0 K, some of the T_2 molecules will be in excited states. At 27 K, the T_2 molecules will be distributed mainly in the first four rotational states of the electronic and vibrational ground state. In fact, more T_2 molecules will be in the $J_i = 1$ state than in $J_i = 0$. Past calculations of the FSD focused mainly on $J_i = 0$ [2,3,14]. Calculations of transitions with $J_i = 1$ were performed [14], but only for the ground state of ${}^3\text{HeT}^+$. We therefore calculated separate FSD's for the ground and electronically excited states of ${}^3\text{HeT}^+$, with T_2 in initial states of $J_i = 1, 2$ and 3.

Eq. (6) was derived for the case when T_2 is in the state $J_i = 0$. For $J_i = 1, 2$, and 3 the relevant equations and derivation are given in the Appendix.

For each of the FSD's, before energy binning was performed, the excitation energies E_f were shifted by the respective rotational excitation energy of the T_2 molecule in order to make the endpoint energies of all the FSD's consistent. Figure 3 shows the Gaussian form of the FSD (in terms of probability density, summed over 1 eV bins) of the ground electronic state of ${}^3\text{HeT}^+$ for the different initial states of T_2 .

D. Isotopes of T_2

In previous tritium β decay experiments the source has had a significant contamination of HT molecules. In Refs. [14] and [15] an elaborate FSD of ${}^3\text{HeH}^+$ was calculated. We have recalculated the FSD of ${}^3\text{HeH}^+$ for HT in states $J_i = 0$ and 1. However in the future KATRIN experiment the T_2 purity will be much higher, with the main contamination expected to come from DT molecules. Therefore the FSD of ${}^3\text{HeD}^+$ has been calculated for DT in initial states $J_i = 0$ and 1. These distributions have not been calculated previously. As will be shown in Sec. IV. C, an uncertainty in the percentage of DT molecules has a significant effect on the reliability of the neutrino mass obtained.

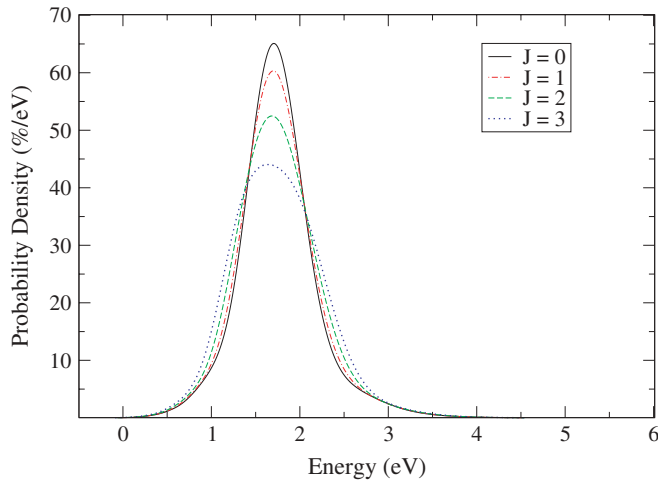


FIG. 3. (Color online) Final state probability density distribution for the electronic ground state of ${}^3\text{HeT}^+$ for initial $J_i = 0, 1, 2$, and 3.

E. Sum rules

To check the accuracy of our calculations we used two sum rules satisfied by P_{nvJ} and $P_{nJ}(E)$. Summing Eq. (6) over v and J , adding the integral of Eq. (7) over J , and using a closure relation gives (see Ref. [35])

$$P_n = \sum_{v,J} P_{nvJ} + \sum_J \int P_{nJ}(E) dE = \int_0^\infty S_n^2(R) [f_{100}^i(R)]^2 dR. \quad (10)$$

Analogously [3],

$$P_{nJ} = \sum_v P_{nvJ} + \int P_{nJ}(E) dE = (2J+1) \int_0^\infty S_n^2(R) j_J^2(KR) [f_{100}^i(R)]^2 dR. \quad (11)$$

These sum rules provide a useful test of our results as they are computed without solving the radial Schrödinger equation of the daughter molecule.

For all J , our errors in P_{nJ} were found to be $< 2 \times 10^{-5}\%$ for the electronic ground state ($n = 1$) and $< 1 \times 10^{-4}\%$ for the electronically excited states ($n = 2-6$). The error in P_n was found to be $< 1 \times 10^{-4}\%$ for $n = 1$, and $< 7 \times 10^{-4}\%$ for $n > 1$.

IV. MODELING

A. Temperature effects

If the source is thermal, the relative populations of rotational states of the T_2 molecules are dependent on the temperature of the source and are given by a Boltzmann distribution. At a temperature of 30 K, the amount of T_2 molecules in states $J_i = 0, 1, 2$, and 3 are 43%, 56%, 1%, and $1 \times 10^{-4}\%$, respectively. The overall FSD at a given temperature is obtained by summing the FSD's for each different initial state J_i , weighted by the percentage of T_2 molecules in that state.

An uncertainty in the temperature of the source could result in an inaccurate FSD being used in the calculation of the theoretical spectrum, and hence an error in the neutrino mass deduced from fitting the theoretical and experimental spectra. To determine how accurately the temperature of the source must be known, we have investigated the effect of uncertainties in the source temperature on the value of the neutrino mass deduced from fitting.

The spectrum obtained by the KATRIN experiment is in fact an integral β decay spectrum. The spectrometer used in the KATRIN experimental setup acts as an integrating high-energy filter. Cylindrical electrodes produce an electrostatic potential that allows only the electrons with enough energy to pass the electrostatic barrier through to the detector. The integrated spectrum, recorded by varying the retarding potential, is given by [22]

$$N(qU) = N_{\text{tot}} t_U \int_0^{W_0} I(E_e) f_{\text{res}}(E_e, qU) dE_e, \quad (12)$$

where U is the retarding potential, N_{tot} is the total number of tritium nuclei in the source and t_U is the measuring time

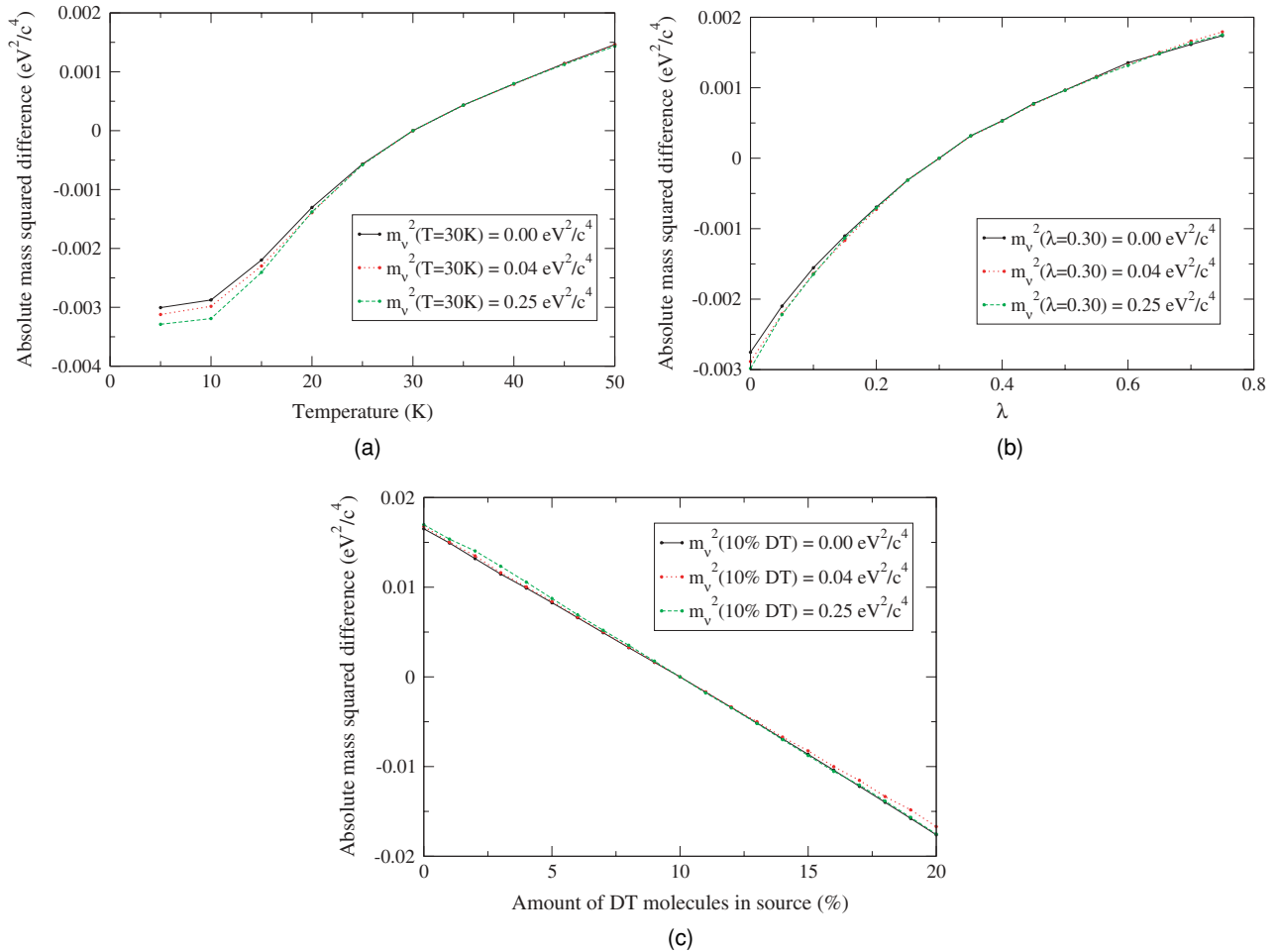


FIG. 4. (Color online) Error in the neutrino mass squared deduced from fitting, due to uncertainties in (a) source temperature (b) ortho-para ratio, and (c) amount of DT molecules in the source (from fitting of β spectrum with $W_0 = 18.6$ keV, $T = 30$ K, and 100% T_2).

at retarding potential U . f_{res} is the response function of the KATRIN spectrometer for isotropically emitted electrons (see Ref. [22]).

The experiments are not free from systematic and statistical errors, therefore these must be accounted for in the theoretical spectra as fit parameters. For an accurate investigation of the temperature uncertainty effects, we would ideally need to include the effect of all these parameters. To obtain an estimate of the error in the neutrino mass caused by uncertainty in source temperature, we have performed fits with idealized conditions (no systematic or statistical errors) and only the fit parameters expected from a theoretical point of view.

To do this we took the FSD for temperature $T = 30$ K and produced a reference integrated β spectrum by using Eq. (12) and chosen values for the fit parameters A , W_0 , and $m_{\bar{\nu}_e}^2$. The endpoint energy, W_0 , was fixed at a value of 18.6 keV, and the normalization constant omitted. We ran separate calculations for three different chosen values of the neutrino mass, 0.0, 0.2, and 0.5 eV. We then fitted theoretical integral β spectra for temperatures in the range 5–50 K, in steps of 5 K, to the reference spectrum with $m_{\bar{\nu}_e}^2$, as the only free parameter. For the fitting we used an energy window with a lower limit of 30 eV below the endpoint, as this will be the energy interval

analyzed in the KATRIN experiment. The last 2 eV below the endpoint was not included in the fitting, as the spectrum here is dominated by the background noise. A statistical distribution for the error in the intensity of β electrons, $\sigma = \sqrt{I}$, was assumed. The mass errors, defined as the absolute difference in $m_{\bar{\nu}_e}^2$, are shown in Fig. 4(a). These absolute differences in $m_{\bar{\nu}_e}^2$ are very similar for all three values of the neutrino mass squared tested. For a 0.2 eV neutrino mass this translates to a $\pm 0.25\%$ error in the value of $m_{\bar{\nu}_e}$, as a result of an uncertainty in the source temperature of ± 5 K. For these calculations a pure tritium source was assumed.

B. Effects of a nonthermal source

For homonuclear molecules with nonzero nuclear spin, transitions between symmetric and antisymmetric states occur so slowly that it may take months or years before a molecule goes from an even-numbered rotational level to an odd-numbered level. Therefore, if the source is initially at a higher (lower) temperature than 30 K and is then cooled (heated) to 30 K, it may take a long time before the source becomes thermal. In this case we may regard the T_2 molecules as a mixture of two separate species, para- T_2 (even J) and

ortho- T_2 (odd J), and use separate partition functions for each species:

$$Q_p(T) = \sum_{J_{\text{even}}} g_J e^{-E_J/kT}, \quad (13a)$$

$$Q_o(T) = \sum_{J_{\text{odd}}} g_J e^{-E_J/kT}, \quad (13b)$$

where $Q_p(T)$ and $Q_o(T)$ are the partition functions for the para and ortho T_2 at temperature T , $g_J = (2J + 1)$ is a rotational degeneracy factor, E_J is the energy of the state with rotational quantum number J with respect to E_0 , and k is Boltzmann's constant.

The total partition function is then given by

$$Q_T = (1 - \lambda)Q_p + (\lambda)Q_o, \quad (14)$$

where λ (which includes spin degeneracy) defines the ortho/para ratio. For thermalized T_2 at $T = 0$ K, λ is 0, and at high temperatures, λ is 3/4.

The relative populations are then

$$P(J_{\text{even}}) = \frac{(1 - \lambda)g_J e^{-E_J/kT}}{Q_T}, \quad (15a)$$

$$P(J_{\text{odd}}) = \frac{\lambda g_J e^{-E_J/kT}}{Q_T}. \quad (15b)$$

We have looked at how the deduced neutrino mass changes with uncertainties in the ortho/para ratio of the source. Using the same fitting procedure as was used for investigating the temperature uncertainty effects, different theoretical integrated spectra for λ varying between 0 and 3/4 in steps of 0.05 were fitted to a reference spectrum for $\lambda = 0.3$ (corresponding to $T = 29.6$ K). The results are shown in Fig. 4(b). The error of the neutrino mass squared is similar to the error caused by temperature uncertainty. KATRIN will use thermalized T_2 , which will be rapidly cooled, so λ values in the range $0.3 < \lambda < 0.75$ are to be expected. It should also be noted that the stability of the ortho- and para- T_2 ratio also depends completely on experimental conditions. The long lifetime stabilization is valid for isolated molecules; however molecular collisions with the walls (and possibly external fields) may very well change these numbers. It is therefore essential that the ortho-para ratio be measured directly when one is running the experiment rather than be obtained from theory.

C. DT contamination

Even though the isotopic purity of tritium in the source of the KATRIN experiment is expected to be at least 95%, this means that the amount of DT molecules may be anything between 0% and 10%. To see how accurately this percentage needs to be known, we have investigated the error in the neutrino mass deduced as a result of uncertainties in the amount of DT in the source between 0% and 20%. We have assumed that the temperature of the source is 30 K. The results of these fits, Fig. 4(c), show that for a neutrino mass of 0.2 eV, a 10% change in the amount of DT molecules in the source gives an error in the deduced neutrino mass of $\approx 22\%$. This is a significant difference, and therefore the isotope contamination

needs to be measured more accurately than the current estimate proposed by the KATRIN experiment.

While performing these various fits, we found that the size of the energy interval below the endpoint chosen in which to perform the fit affected the estimated error in the neutrino mass deduced. We considered energies within the range of 10–30 eV below the endpoint. However, this is not a major issue for our fits, as we are simply studying the sensitivity of various experimental parameters to the makeup of the tritium source. More precise error estimates can be performed by using our data once the precise experimental parameters and, in particular, the range of energies to be fitted are known.

V. CONCLUSION

We have calculated the final state distributions of the six lowest lying electronic states of ${}^3\text{HeT}^+$, ${}^3\text{HeD}^+$, and ${}^3\text{HeH}^+$ resulting from the β decay of T_2 , DT, and HT to accommodate the increased sensitivity and requirements of the future neutrino mass experiments. We have investigated the effect of rotational excitations of the parent molecules by explicitly calculating separate final state distributions for the daughter molecules following the β decay of T_2 in rotational states $J_i = 0, 1, 2$, and 3, and DT/HT in states $J_i = 0$ and 1.

We have obtained estimates of the error in the value of the neutrino mass deduced from fitting theoretical curves, due to uncertainties in the temperature, ortho-para ratio, and percentage of DT molecules in the source in order to see how accurately these need to be known. Our results show that uncertainties in the (rotational) temperature and ortho-para ratio are less of a problem than those in deuterium fraction. It is recommended that the amount of DT molecules is determined in the source, for example by using spectroscopy, after cooling.

ACKNOWLEDGMENTS

We thank Klaus Eitel and other members of the KATRIN collaboration for helpful discussions.

APPENDIX

The probability of finding the daughter ion in a final state Ψ^f following the β decay of the parent molecule in an initial state Ψ^i is

$$P_{if} = |\langle \Psi^f | e^{i\mathbf{K}\cdot\mathbf{R}} | \Psi^i \rangle|^2 = \left| \int \Psi^{f*} e^{i\mathbf{K}\cdot\mathbf{R}} \Psi^i d\mathbf{R} \right|^2, \quad (A1)$$

where $\mathbf{K} = -\mathbf{p}_e m_T / (m_T + m_{\text{He}} + 2m_e) \hbar$, \mathbf{R} is the internuclear distance, and Ψ^i and Ψ^f are functions of relative coordinates only.

Invoking the adiabatic approximation for Ψ^i and Ψ^f gives

$$\Psi^i = \psi_{n_i}^i(r_1, r_2; R) R^{-1} f_{n_i v_i J_i}^i(R) Y_{J_i M_i}(\theta, \phi), \quad (A2a)$$

$$\Psi^f = \psi_n^f(r_1, r_2; R) R^{-1} f_{n v J}^f(R) Y_{JM}(\theta, \phi). \quad (A2b)$$

ψ_n are the clamped-nuclei electronic wave functions, $f_{n v J}$ are the radial vibrational wave functions, Y_{JM} are the spherical harmonics, r_1 and r_2 denote the spatial positions of the electrons, (R, θ, ϕ) are the spherical coordinates of \mathbf{R} , and

n, v, J and M are the electronic, vibrational, rotational, and azimuthal quantum numbers.

From the standard partial wave expansion for $e^{i\mathbf{K}\cdot\mathbf{R}}$,

$$e^{i\mathbf{K}\cdot\mathbf{R}} = 4\pi \sum_{l=0}^{\infty} \sum_{m=-l}^{+l} i^l j_l(KR) Y_{lm}^*(\theta_K, \phi_K) Y_{lm}(\theta, \phi), \quad (\text{A3})$$

where $j_l(KR)$ is the spherical Bessel function, (K, θ_K, ϕ_K) are the spherical components of \mathbf{K} , and

$$d\mathbf{R} = R^2 d\Omega_R dR, \quad (\text{A4})$$

the integration can be reduced to

$$P_{nvJM}(K) = (4\pi)^2 \left| \sum_{lm} Y_{lm}^*(\theta_K, \phi_K) \int S_n(R) f_{nvJ}^{f*}(R) \times f_{n_i v_i J_i}^i(R) j_l(KR) dR \int Y_{JM}^*(\theta, \phi) \times Y_{lm}(\theta, \phi) Y_{J_i M_i}(\theta, \phi) d\Omega_R \right|^2, \quad (\text{A5})$$

where $S_n(R)$ is the overlap integral providing the R -dependent probability amplitude of transition to the n^{th} electronic state of the daughter system and is given by

$$S_n(R) = \int \psi_n^{f*}(r_1, r_2; R) \psi_{n_i}^i(r_1, r_2; R) dr_1 dr_2. \quad (\text{A6})$$

Averaging over initial M_i , summing over final M , and averaging over final directions K gives

$$P_{nvJ}(K) = \frac{4\pi}{(2J_i + 1)} \sum_{MM_i} \times \int \sum_{lm'l'm'} Y_{lm}^*(\theta_K, \phi_K) Y_{l'm'}(\theta_K, \phi_K) d\Omega_K \times \left| \int S_n(R) f_{nvJ}^{f*}(R) f_{n_i v_i J_i}^i(R) j_l(KR) dR \right|^2 \times \left| \int Y_{JM}^*(\theta, \phi) Y_{lm}(\theta, \phi) Y_{J_i M_i}(\theta, \phi) d\Omega_R \right|^2. \quad (\text{A7})$$

Since

$$\int Y_{lm}^*(\theta_K, \phi_K) Y_{l'm'}(\theta_K, \phi_K) d\Omega_K = \delta_{ll'} \delta_{mm'}, \quad (\text{A8})$$

one has

$$P_{nvJ}(K) = \frac{4\pi}{(2J_i + 1)} \sum_l \sum_{MmM_i} \times \left| \int Y_{JM}^*(\theta, \phi) Y_{lm}(\theta, \phi) Y_{J_i M_i}(\theta, \phi) d\Omega_R \right|^2 \times \left| \int S_n(R) f_{nvJ}^{f*}(R) f_{n_i v_i J_i}^i(R) j_l(KR) dR \right|^2. \quad (\text{A9})$$

The integration over three spherical harmonics can be represented in terms of matrix elements:

$$\int Y_{JM}^*(\theta, \phi) Y_{lm}(\theta, \phi) Y_{J_i M_i}(\theta, \phi) d\Omega_R = \langle JM | Y_{lm} | J_i M_i \rangle. \quad (\text{A10})$$

The Wigner-Eckart theorem for the factorization of the matrix elements of tensor operators is

$$\langle j'm' | \mathbf{T}(kq) | jm \rangle = (-1)^{j'-m'} \begin{pmatrix} j' & k & j \\ -m' & q & m \end{pmatrix} \langle j' || \mathbf{T}_k || j \rangle, \quad (\text{A11})$$

where $\mathbf{T}(kq)$ is a tensor operator of rank k . The theorem states that the dependence of the matrix element $\langle j'm' | \mathbf{T}(kq) | jm \rangle$ on the projection quantum numbers is entirely contained in the Wigner $3j$ -symbol. $\langle j' || \mathbf{T}_k || j \rangle$ are the reduced matrix elements.

The total transition probability (summed over magnetic quantum numbers) is therefore

$$\sum_{m'qm} |\langle j'm' | \mathbf{T}(kq) | jm \rangle|^2 = |\langle j' || \mathbf{T}_k || j \rangle|^2 \sum_{m'qm} \begin{pmatrix} j' & k & j \\ -m' & q & m \end{pmatrix}^2 = |\langle j' || \mathbf{T}_k || j \rangle|^2. \quad (\text{A12})$$

The orthogonality property of $3j$ -symbols has been used and is given by

$$\sum_{\alpha\beta} \begin{pmatrix} a & b & c \\ \alpha & \beta & \gamma \end{pmatrix} \begin{pmatrix} a & b & c' \\ \alpha & \beta & \gamma' \end{pmatrix} = \frac{1}{(2c+1)} \delta_{cc'} \delta_{\gamma\gamma'} \delta(abc), \quad (\text{A13})$$

where $\delta(abc) = 1$ if a, b, c satisfy the triangular condition

$$|a-b| \leq c \leq |a+b| \quad (\text{A14})$$

and is zero otherwise.

Therefore one gets

$$\sum_{MmM_i} \left| \int Y_{JM}^*(\theta, \phi) Y_{lm}(\theta, \phi) Y_{J_i M_i}(\theta, \phi) d\Omega_R \right|^2 = |\langle J || Y_l || J_i \rangle|^2. \quad (\text{A15})$$

The reduced matrix elements of spherical harmonics are given by

$$\langle j' || Y_k || j \rangle = (-1)^{j'} \left[\frac{(2j'+1)(2k+1)(2j+1)}{4\pi} \right]^{\frac{1}{2}} \begin{pmatrix} j' & k & j \\ 0 & 0 & 0 \end{pmatrix}, \quad (\text{A16})$$

hence

$$|\langle J || Y_l || J_i \rangle|^2 = \frac{(2J+1)(2l+1)(2J_i+1)}{4\pi} \begin{pmatrix} J & l & J_i \\ 0 & 0 & 0 \end{pmatrix}^2. \quad (\text{A17})$$

A $3j$ symbol with $m_1 = m_2 = m_3 = 0$ can be computed by using the general formula

$$\begin{pmatrix} j_1 & j_2 & j_3 \\ 0 & 0 & 0 \end{pmatrix} = \left[\frac{(J-2j_1)!(J-2j_2)!(J-2j_3)!}{(J+1)!} \right]^{1/2} \times \frac{\frac{J!}{2!}}{\left(\frac{J}{2}-j_1\right)!\left(\frac{J}{2}-j_2\right)!\left(\frac{J}{2}-j_3\right)!}, \quad (\text{A18})$$

where $J = j_1 + j_2 + j_3$. J must be even, otherwise the $3j$ symbol equals 0.

The angular momentum algebra [Eqs. (A10)–(A18)] was obtained from Refs. [36,37].

To obtain a final equation for the probability, one needs to evaluate Eqs. (A17) and (A18) for different values of J_i .

For $J_i = 0$: From the triangular condition and the fact that $a + b + c$ must be even, $l = J$. Therefore:

$$\begin{aligned} |\langle J \| Y_l \| J_i \rangle|^2 &= |\langle J \| Y_J \| 0 \rangle|^2 \delta_{l,J} \\ &= \frac{(2J+1)(2J+1)}{4\pi} \begin{pmatrix} J & J & 0 \\ 0 & 0 & 0 \end{pmatrix}^2 \delta_{l,J}, \quad (\text{A19}) \end{aligned}$$

$$|\langle J \| Y_J \| 0 \rangle|^2 = \frac{2J+1}{4\pi} \delta_{l,J}. \quad (\text{A20})$$

Substituting this back into Eq. (A9) gives (as stated in Ref. [14]):

$$P_{nvJ}(K) = (2J+1) \left| \int S_n(R) f_{nvJ}^f{}^*(R) f_{n_i v_i 0}^i(R) j_J(KR) dR \right|^2. \quad (\text{A21})$$

For $J_i = 1$: Here $l = J \pm 1$.

$$|\langle J \| Y_l \| J_i \rangle|^2 = |\langle J \| Y_{J+1} \| 1 \rangle|^2 \delta_{l,J+1} + |\langle J \| Y_{J-1} \| 1 \rangle|^2 \delta_{l,J-1}, \quad (\text{A22})$$

$$|\langle J \| Y_l \| 1 \rangle|^2 = \frac{3}{4\pi} [(J+1)\delta_{l,J+1} + J\delta_{l,J-1}]. \quad (\text{A23})$$

Therefore [14]

$$\begin{aligned} P_{nvJ}(K) &= (J+1) \left| \int S_n(R) f_{nvJ}^f{}^*(R) f_{n_i v_i 1}^i(R) j_{J+1}(KR) dR \right|^2 \\ &\quad + J \left| \int S_n(R) f_{nvJ}^f{}^*(R) f_{n_i v_i 1}^i(R) j_{J-1}(KR) dR \right|^2. \quad (\text{A24}) \end{aligned}$$

For $J_i = 2$: We have $l = J \pm 2$ and $l = J$

$$\begin{aligned} |\langle J \| Y_l \| J_i \rangle|^2 &= |\langle J \| Y_{J+2} \| 2 \rangle|^2 \delta_{l,J+2} + |\langle J \| Y_J \| 2 \rangle|^2 \delta_{l,J} \\ &\quad + |\langle J \| Y_{J-2} \| 2 \rangle|^2 \delta_{l,J-2}, \quad (\text{A25}) \end{aligned}$$

$$\begin{aligned} |\langle J \| Y_l \| 2 \rangle|^2 &= \frac{5}{4\pi} \left[\frac{3(J+2)(J+1)}{2(2J+3)} \delta_{l,J+2} \right. \\ &\quad \left. + \frac{(J+1)J(2J+1)}{(2J+3)(2J-1)} \delta_{l,J} + \frac{3J(J-1)}{2(2J-1)} \delta_{l,J-2} \right]. \quad (\text{A26}) \end{aligned}$$

Therefore

$$\begin{aligned} P_{nvJ}(K) &= \frac{3(J+2)(J+1)}{2(2J+3)} \\ &\quad \times \left| \int S_n(R) f_{nvJ}^f{}^*(R) f_{n_i v_i 2}^i(R) j_{J+2}(KR) dR \right|^2 \\ &\quad + \frac{(J+1)J(2J+1)}{(2J+3)(2J-1)} \\ &\quad \times \left| \int S_n(R) f_{nvJ}^f{}^*(R) f_{n_i v_i 2}^i(R) j_J(KR) dR \right|^2 \\ &\quad + \frac{3J(J-1)}{2(2J-1)} \\ &\quad \times \left| \int S_n(R) f_{nvJ}^f{}^*(R) f_{n_i v_i 2}^i(R) j_{J-2}(KR) dR \right|^2. \quad (\text{A27}) \end{aligned}$$

For $J_i = 3$: $l = J \pm 3$ and $l = J \pm 1$,

$$\begin{aligned} |\langle J \| Y_l \| J_i \rangle|^2 &= |\langle J \| Y_{J+3} \| 3 \rangle|^2 \delta_{l,J+3} + |\langle J \| Y_{J+1} \| 3 \rangle|^2 \delta_{l,J+1} \\ &\quad + |\langle J \| Y_{J-1} \| 3 \rangle|^2 \delta_{l,J-1} \\ &\quad + |\langle J \| Y_{J-3} \| 3 \rangle|^2 \delta_{l,J-3}, \quad (\text{A28}) \end{aligned}$$

$$\begin{aligned} |\langle J \| Y_l \| 3 \rangle|^2 &= \frac{7}{4\pi} \left[\frac{5(J+3)(J+2)(J+1)}{2(2J+5)(2J+3)} \delta_{l,J+3} \right. \\ &\quad + \frac{3(J+2)(J+1)J}{2(2J+5)(2J-1)} \delta_{l,J+1} \\ &\quad + \frac{3(J+1)J(J-1)}{2(2J+3)(2J-3)} \delta_{l,J-1} \\ &\quad \left. + \frac{5J(J-1)(J-2)}{2(2J-1)(2J-3)} \delta_{l,J-3} \right]. \quad (\text{A29}) \end{aligned}$$

Therefore

$$\begin{aligned} P_{nvJ}(K) &= \frac{5(J+3)(J+2)(J+1)}{2(2J+5)(2J+3)} \\ &\quad \times \left| \int S_n(R) f_{nvJ}^f{}^*(R) f_{n_i v_i 3}^i(R) j_{J+3}(KR) dR \right|^2 \\ &\quad + \frac{3(J+2)(J+1)J}{2(2J+5)(2J-1)} \\ &\quad \times \left| \int S_n(R) f_{nvJ}^f{}^*(R) f_{n_i v_i 3}^i(R) j_{J+1}(KR) dR \right|^2 \\ &\quad + \frac{3(J+1)J(J-1)}{2(2J+3)(2J-3)} \\ &\quad \times \left| \int S_n(R) f_{nvJ}^f{}^*(R) f_{n_i v_i 3}^i(R) j_{J-1}(KR) dR \right|^2 \\ &\quad + \frac{5J(J-1)(J-2)}{2(2J-1)(2J-3)} \\ &\quad \times \left| \int S_n(R) f_{nvJ}^f{}^*(R) f_{n_i v_i 3}^i(R) j_{J-3}(KR) dR \right|^2. \quad (\text{A30}) \end{aligned}$$

- [1] W. Kołos, B. Jeziorski, K. Szalewicz, and H. J. Monkhorst, *Phys. Rev. A* **31**, 551 (1985).
- [2] O. Fackler, B. Jeziorski, W. Kołos, H. J. Monkhorst, and K. Szalewicz, *Phys. Rev. Lett.* **55**, 1388 (1985).
- [3] B. Jeziorski, W. Kołos, K. Szalewicz, O. Fackler, and H. J. Monkhorst, *Phys. Rev. A* **32**, 2573 (1985).
- [4] W. Kołos, B. Jeziorski, H. J. Monkhorst, and K. Szalewicz, *Int. J. Quantum Chem.* **S19**, 421 (1986).
- [5] K. Szalewicz, O. Fackler, B. Jeziorski, W. Kołos, and H. J. Monkhorst, *Phys. Rev. A* **35**, 965 (1987).
- [6] P. Froelich, K. Szalewicz, B. Jeziorski, W. Kołos, and H. J. Monkhorst, *J. Phys. B* **20**, 6173 (1987).
- [7] W. Kołos, B. Jeziorski, J. Rychlewski, K. Szalewicz, H. J. Monkhorst, and O. Fackler, *Phys. Rev. A* **37**, 2297 (1988).
- [8] P. Froelich, B. Jeziorski, W. Kołos, H. Monkhorst, A. Saenz, and K. Szalewicz, *Phys. Rev. Lett.* **71**, 2871 (1993).
- [9] S. Jonsell and H. J. Monkhorst, *Phys. Rev. Lett.* **76**, 4476 (1996).
- [10] P. Froelich and A. Saenz, *Phys. Rev. Lett.* **77**, 4724 (1996).
- [11] A. Saenz and P. Froelich, *Phys. Rev. C* **56**, 2132 (1997).
- [12] A. Saenz and P. Froelich, *Phys. Rev. C* **56**, 2162 (1997).
- [13] S. Jonsell, A. Saenz, and P. Froelich, *Pol. J. Chem.* **72**, 1323 (1998).
- [14] S. Jonsell, A. Saenz, and P. Froelich, *Phys. Rev. C* **60**, 034601 (1999).
- [15] A. Saenz, S. Jonsell, and P. Froelich, *Phys. Rev. Lett.* **84**, 242 (2000).
- [16] C. Weinheimer *et al.*, *Phys. Lett.* **B460**, 219 (1999).
- [17] V. M. Lobashev *et al.*, *Phys. Lett.* **B460**, 227 (1999).
- [18] C. Kraus *et al.*, *Eur. Phys. J. C* **40**, 447 (2005).
- [19] V. M. Lobashev, *Nucl. Phys.* **A719**, 153 (2003).
- [20] A. Osipowicz *et al.*, FZKA scientific report 6691 hep-ex/0109033 (2001).
- [21] T. Thümmeler *et al.*, FZKA scientific report 6752 (2002).
- [22] J. Angrik *et al.*, FZKA scientific report 7090 (2005).
- [23] M. Cantwell, *Phys. Rev.* **101**, 1747 (1956).
- [24] R. J. Le Roy, University of Waterloo Chemical Physics Research Report **CP-555R** (1996).
- [25] R. J. Le Roy, *Comput. Phys. Commun.* **52**, 383 (1989).
- [26] W. Kołos, *Int. J. Quantum Chem.* **10**, 217 (1976).
- [27] W. Kołos and J. M. Peek, *Chem. Phys.* **12**, 381 (1976).
- [28] D. M. Bishop and L. M. Cheung, *J. Mol. Spectrosc.* **75**, 462 (1979).
- [29] L. Wolniewicz, *J. Chem. Phys.* **99**, 1851 (1993).
- [30] J. A. Coxon and P. G. Hajigeorgiou, *J. Mol. Spectrosc.* **193**, 306 (1999).
- [31] A. Carrington, R. A. Kennedy, T. P. Softley, P. G. Fournier, and E. G. Richard, *Chem. Phys.* **81**, 251 (1983).
- [32] M. W. Crofton, R. S. Altman, N. N. Haese, and T. Oka, *J. Chem. Phys.* **91**, 5882 (1989).
- [33] F. Matsushima, T. Oka, and K. Takagi, *Phys. Rev. Lett.* **78**, 1664 (1997).
- [34] E. A. Engel, N. Doss, G. J. Harris, and J. Tennyson, *Mon. Not. R. Astron. Soc.* **357**, 471 (2005).
- [35] L. Wolniewicz, *J. Chem. Phys.* **43**, 1087 (1965).
- [36] A. R. Edmonds, *Angular Momentum in Quantum Mechanics* (Princeton University Press, Princeton, N.J., 1996).
- [37] D. M. Brink and G. R. Satchler, *Angular Momentum* (Oxford University Press, New York, 1979).